Soriano Amat, M., Martins, H.F., Durán, V., Fermoso, P., Martín López, S., González Herráez, M. & Fernández Ruiz, M.R. 2023, "Frequency stability requirements in quasi-integer-ratio time-expanded phase-sensitive OTDR", Journal of Lightwave Technology, vol. 41, no. 2, pp. 777-783.

Available at http://dx.doi.org/10.1109/JLT.2022.3217651

Frequency stability requirements in quasi-integer-ratio time-expanded phase-sensitive OTDR

Miguel Soriano-Amat, Hugo F. Martins, Vicente Durán, Pablo Fermoso, Sonia Martin-Lopez, Miguel Gonzalez-Herraez, María R. Fernández-Ruiz,

***Abstract*— Time-expanded phase sensitive (TE-φ)OTDR is a recently reported technique for distributed fiber sensing that relies on the use of an electro-optic dual frequency comb (DFC) scheme. A distinctive feature of this approach is its ability to provide high spatial resolution (on the centimeter scale) with detection bandwidths orders of magnitude lower than those of conventional φOTDR systems. The stringent trade-off between resolution, range and sensing bandwidth that exists in TE-φ OTDR has demonstrated to be substantially relaxed by implementing two frequency combs with quasi-integer-ratio repetition rates. However, employing very dissimilar line separations (with a ratio between them > 100) is challenging due to the need of keeping the coherence over long sequences of interferograms, which eventually limits the attainable range. In this paper, we formulate the requirements for the frequency stability of the reference clock used in a quasi-integer-ratio DFC scheme. This analysis allows us to stablish the limits on the number of comb lines (i.e., on the number of available independent sensing points) for a particular reference clock. By using a rubidium atomic clock (with a relative frequency stability of ~10^{-13}), we demonstrate up to 10^5 sensing points along 2 km of fiber with tens of Hz sensing bandwidth.**

***Index Terms*—Dual frequency comb, modulation coding, optical time-domain reflectometry, scattering Rayleigh, quasi-integer-ratio.**

This work was supported in part by Comunidad de Madrid and FEDER Program under Grant SINFOTON2-CM: S2018/NMT-4326, Generalitat Valenciana (PROMETEO/2020/029) and the Universitat Jaume I (UJI-B2019-45). Also, this work has been partially funded by the Spanish MCIN/AEI/ 10.13039/ 501100011033 and by the European Union NextGenerationEU/PRTR program, under project PSI ref. PLEC2021-007875, and by the Spanish MCIN/AEI/ 10.13039/ 501100011033 and FEDER "Una manera de hacer Europa" under Projects RTI2018-097957-B-C31, RTI2018-097957-B-C32, RTI2018-097957-B-C33, PID2021-128000OB-C21 and PID2021-128000OB-C22.

Miguel Soriano-Amat, Pablo Fermoso, Sonia Martin-Lopez, Miguel Gonzalez-Herraez and are with the Universidad de Alcalá, Departamento de Electrónica, 28805 Alcalá de Henares, Spain, (e-mail: miguel.soriano@uah.es, pablo.fermoso@uah.es; sonia.martinlo@uah.es; miguel.gonzalezh@uah.es).

Hugo F. Martins is with the Instituto de Óptica "Daza de Valdés", IO-CSIC, 28006 Madrid, Spain (e-mail: hugo.martins@csic.es).

Vicente Duran is with the GROC-UJI, Institute of New Imaging Technologies, University Jaume I, 120071 Castellón, Spain (e-mail: vduran@uji.es).

María R. Fernández-Ruiz is with the Universidad de Alcalá, Departamento de Electrónica, 28805 Alcalá de Henares, Spain and with the Instituto de Óptica "Daza de Valdés", IO-CSIC, 28006 Madrid, Spain (rosario.fernandezr@uah.es).

I. Introduction

Distributed acoustic sensing (DAS) is a technique attracting a great deal of attention in a broad variety of fields, including civil engineering, security, surveillance, and seismology, among others [1]–[3]. DAS offers interesting features unmatched by any other sensing technology, such as long range remote sensing with high spatial resolution and acoustic sampling rates (up the kHz regime). In particular, state-of-the-art DAS attains ranges of tens of km with resolutions of several meters (even overcoming 100 km when assisted with distributed amplification [4], [5]), thus providing around 10,000 independent sensing points, with a sampling rate only limited by the fiber length (e.g., 2 kHz for a range of 50 km).

In a conventional DAS system, optical pulses are launched into an optical fiber to originate Rayleigh backscattering. The returning signal is detected and analyzed to extract information about strain or temperature perturbations in the surroundings of the fiber. This scheme has a well-known trade-off between spatial resolution (fixed by the probe optical bandwidth) and the signal-to-noise ratio (SNR) of the measured traces. To overcome this issue, researchers have proposed the use of pulse coding techniques [6]–[8], thanks to which centimeter resolutions over kilometer ranges are achieved. However, for such a fine resolution, the bandwidth of the probe pulses must reach several gigahertz, with the subsequent increase of the photodetection bandwidth requirements and, hence, of the cost. Besides, broader photo-detection bandwidth not only induces higher noise, impairing the attainable SNR, but also leads to the need of higher capacity acquisition cards, producing a massive amount of data. For example, a DAS sensor with spatial resolution of 2 cm would need a photodetection bandwidth of at least 5 GHz. The acquisition card should then have a minimum sampling rate of 10 GSps, which leads to a data rate of 80 GBps, assuming double-precision floating-point valued samples.

Recently, we have proposed a novel distributed sensing technique, termed as time-expanded phase sensitive OTDR (TE-φOTDR), to significantly reduce the photo-detection bandwidth requirements in high spatial resolution φOTDR sensors [9]. This technique employs a dual frequency comb

scheme, i.e., two similar frequency combs with a slight detuning in their repetition rates [10]. One comb is used as the probe signal to be launched into the fiber, while the other comb acts as local oscillator (LO) for coherent mixing with the Rayleigh backscattered signal. Upon detection, an optical-to-radio frequency (RF) downconversion is produced, reducing the signal bandwidth in several orders of magnitude. In [9], 2 cm spatial resolution was attained with a photo-detection bandwidth of only 200 kHz, which corresponds to a data rate well below 10 MBps, that is, four orders of magnitude lower than that of a traditional φOTDR with the same spatial resolution. As in any other dual-comb-based scheme, a drawback of TE-φOTDR is related to the need of avoiding aliasing between beat frequencies in detection. This requirement involves to accomplish the relationship $\delta f < f_R^2/(2B_o)$, where δf is the offset between the combs' repetition rates, f_R is the repetition rate of the slower comb and B_o is the combs' optical bandwidth [9], [10]. Writing this expression in terms of some parameters of the sensor yields:

$$f_S < \frac{c}{4n}\frac{\Delta z}{L_{\max}^2} \tag{1}$$

where $f_S = \delta f$ is the sensing sampling rate, $\Delta z = c/(2nB_o)$ is the spatial resolution, $L_{\max} = c/(2nf_R)$ is the maximum fiber length that can be interrogated, c is the speed of light in a vacuum and n is the effective refractive index of the fiber. Hence, this technique imposes a stringent trade-off between three fundamental performance parameters of the sensor system. In [9], an approach to relax this condition was briefly introduced, based on the use of a scheme that employs two combs with quasi-integer-ratio (QIR) repetition rates [11], which henceforth we will abbreviate as QIR-TE-φOTDR. In this approach, a comb of sampling rate f_R is used as probe to interrogate the optical fiber, while a faster comb of sampling rate $M \cdot f_R + \delta f$ is used as LO, being M a positive integer ($M > 1$). Hence, if the probe comb has N lines, the LO comb has P lines, being $P \simeq N/M$. Similarly to the original case, a multiheterodyne process occurs upon detection but instead of having a one-to-one relationship between probe and LO lines, in this case the p th line of the LO acts as a reference for the $[(p-1)M+1, pM]$ lines of the probe comb, where the square brackets refers to the limits of a closed interval. By using this technique, the trade-off between sampling rate, resolution and range is relaxed by a factor of M, i.e., $f_S < M \cdot k \cdot \Delta z / L_{\max}^2$, with $k = c/(4n)$. In return, the photo-detection bandwidth is increased in at least a factor of M due to the need for detecting up to M Nyquist zones [9]. Still, the detection bandwidth requirements stay much lower than in conventional φOTDR. Using this configuration with $M = 50$, an optical fiber of 1 km was interrogated with 4 cm resolution and a sampling frequency of 40 Hz, attaining up to 25,000 independent sensing points acquired at a bit rate below 25 MBps [9].

The sliced multiheterodyne process in QIR-TE-φOTDR induces a disordering of probe comb lines in RF domain. In accordance to Fig. 1 ($M = 4$), the offset of the n th line of the probe comb from the baseband is $(\mathrm{mod}(M-n, M)) \cdot f_R + p \cdot \delta f$, where mod is the remainder after division of $(M-n)$ and M. To recover the spatial information correctly, it is required to re-arrange the comb lines, a process that is equivalent to a re-ordering of the samples in the time-domain interferograms. As we will show in the following section, this re-ordering process leads to lines closer to baseband having higher phase noise than in a traditional ($M = 1$) DFC beating process. This increases the impact of phase noise on the temporal traces after the reordering of lines.

In this Article, we thoroughly analyze the effect of the frequency stability requirements of the QIR-TE-φOTDR technique. By using a highly stable RF synthesizer, we experimentally demonstrate QIR-TE-φOTDR for two cases. In the first one, we interrogate a 500 m fiber with 25,000 independent sensing points and a sampling frequency of 1 kHz. In the second case, the length of the fiber will be extended to 2 km, with up to 100,000 independent sensing points and a sampling frequency of 80 Hz. Both measurements requires an acquisition rate equal or below 400 MBps, attaining a reduction of two orders of magnitude with respect to a traditional φOTDR system with the same spatial resolution. The number of achieved sensing points in the two measurements results reported in this article has been increased by a factor of 4 (1) for the first dataset (second dataset) while the sampling frequency is twice (multiplied by 25) when compared to the best results of QIR-TE-φOTDR reported so far in the literature [9].

II. Model of Frequency Stability Requirements in QIR-TE-φOTDR

We start here by providing a model of the comb stability requirements for a successful measurement in QIR-TE-φOTDR. To date, the combs employed in TE-φOTDR configurations have been generated by an electro-optic (EO) modulation scheme [9], [12], [13]. In EO-DFC, there are three main stochastic noise sources that can degrade the signal fidelity, namely, optical noise associated to the laser noise and optical amplifiers, electrical noise added during the comb generation process, and photodiode noise [14]. It has been demonstrated that, in general, the dual comb configuration is particularly sensitive to the relative phase noise between the two frequency combs [15]. The instantaneous frequency of the comb lines depends on the instantaneous frequency of the laser, $\upsilon_0(t)$, and the instantaneous repetition rate of the comb generators ($\upsilon_{probe}(t)$ and $\upsilon_{LO}(t)$, respectively). Hence, the frequency noise of the n th (p th) comb line of the probe (LO) is given by

$$\upsilon_{probe,n}(t) = \upsilon_0(t) + n\upsilon_{probe}(t), \tag{2}$$

$$\upsilon_{LO,p}(t) = \upsilon_0(t) + p\upsilon_{LO}(t). \quad (3)$$

The laser frequency noise can be cancelled in photo-detection if the optical path length difference between the two combs is significantly shorter than the coherence length of the laser. In this work, the laser used has a linewidth of 100 Hz, which implies a coherence length much longer than the probed fiber length. Thus, in this case, the frequency noise is solely given by the relative frequency noise between the two combs. Now, let us assume that the two combs are synthesized from a common oscillator (e.g., through a phase locked loop). Then, the standard deviation of frequency noise of each comb line is proportional to its instantaneous frequency and the relative frequency error of the reference oscillator, ζ_{clock}. In the frequency domain, those expressions can be written as

$$\sigma_{probe,n} = n \cdot f_R \cdot \zeta_{clock} + n \cdot \sigma_{u,probe} \quad (4)$$

$$\sigma_{LO,p} = p\left(M \cdot f_R + \delta f\right)\zeta_{clock} + p \cdot \sigma_{u,\mathrm{LO}} \quad (5)$$

where σ_u stands for the standard deviation of uncorrelated frequency noise terms of each signal. Upon photodetection, the standard deviation of frequency noise of the nth downcoverted probe line (beaten with its corresponding pth LO line) is

$$\sigma_{\mathrm{RF},n} = \left(\mathrm{mod}\left(M-n, M\right) f_R + p\delta f\right)\zeta_{clock} + n \cdot \sigma_{u,probe} + p \cdot \sigma_{u,LO} \quad (6)$$

For low offset values, the main contribution to the frequency noise of a probe tone is due to the first term of eq. (6) [14]. After reordering the RF probe tones, the comb lines have a frequency noise whose magnitude follows a saw-tooth trend with period M (see Fig. 1). The relative frequency uncertainty of each line is obtained from the division between the absolute frequency noise and the final instantaneous frequency of each line,

$$\xi_n = \frac{\left(\mathrm{mod}\left(M-n, M\right) f_R + p\delta f\right)\zeta_{clock}}{n\delta f} \quad (7)$$

Considering $M \gg 1, N \gg 1$ and a fill factor of the Nyquist zones close to 1 (i.e., $\delta f = M f_R^2 / (2B_o)$) we can establish an upper bound for the relative frequency uncertainty as

$$\xi_n < \frac{M f_R}{\delta f}\zeta_{clock} = 2N\zeta_{clock} \quad (8)$$

The integrated jitter along the fiber length would be

$$\Delta T = \frac{1}{(\delta f)^2}\sigma_{\mathrm{RF},n} = \frac{\left(\mathrm{mod}\left(M-n, M\right) f_R + p\delta f\right)\zeta_{clock}}{(\delta f)^2} \quad (9)$$

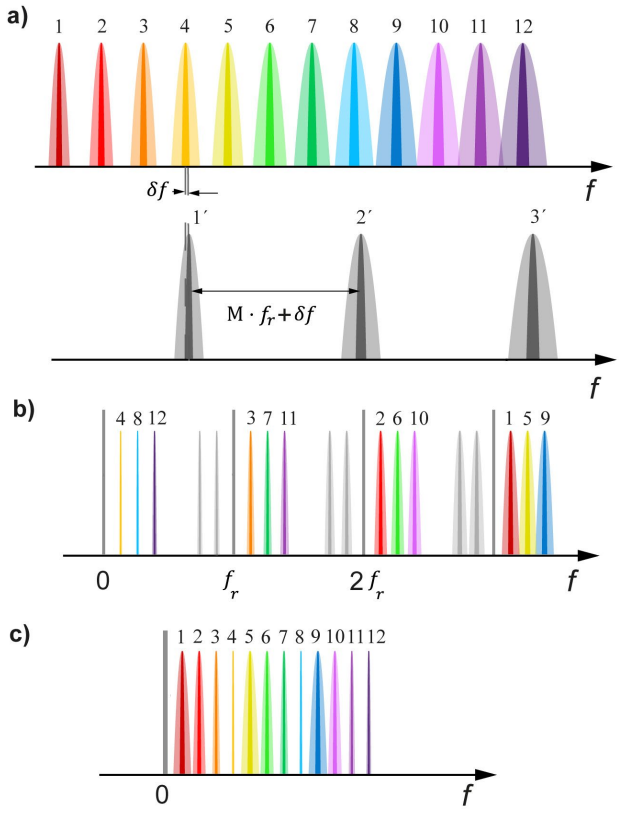

Fig. 1.(a) Probe comb (upper) and local oscillator comb (bottom) with quasi-integer ratio repetition rates ($M = 4$). (b) Spectral lines in RF domain after detection of the beating between dual comb (c) Spectral lines in RF domain after being reordered.

The upper bound for the integrated jitter would be

$$\Delta T_{\max} = \frac{2N}{\delta f}\zeta_{clock} \quad (10)$$

To establish a limit to the maximum frequency error that we can afford in a measurement, we consider that the integrated jitter should be much lower than the duration of one measurement point. This duration is given by $1/(N \cdot \delta f)$. Introducing this condition in eq. (10), we attain the condition for the frequency stability of the clock in QIR- TE-φOTDR,

$$\zeta_{clock} \ll \frac{1}{2N^2} \quad (11)$$

In the original TE-φOTDR system ($M = 1$), each line in RF domain appears ordered. Hence, the relative frequency uncertainty is $\xi_n = \zeta_{clock}$ and the required frequency stability of the clock is given by $\zeta_{clock} \ll 1/N$. The physical meaning of the increase of the requirement for the frequency stability by a factor of $2N$ is related to the fact that beat lines that appear nearly at the upper edge of the RF spectrum must be reordered to be at the lower edge (close to baseband, as depicted in Fig. 1). The upper-frequency limit of the spectrum corresponds to $2N$ times the sampling frequency (δf) when we work with the samples at the odd-order Nyquist zones. In other words, some low-frequency components in the re-ordered comb

spectrum have $2N$ larger frequency noise than in the conventional TE-φOTDR scheme. Since generally the number of points is also larger in QIR-TE-φOTDR than in conventional TE-φOTDR, it appears necessary to pay particular attention to the clock noise in the QIR-TE-φOTDR configuration. Conventional clocks used in laboratory instruments are typically Oven-Controlled Crystal Oscillators (OCXO) with relative stabilities in the order of 10^{-9}. Considering the analysis above, this appears as insufficient to reach the number of resolved points (100,000) targeted in this paper.

III. Experimental Demonstration

Next, we validate our theoretical formulation of the frequency stability condition for QIR-TE-φOTDR by performing two measurements of controlled periodical strain perturbations with different sensing performance.

A. Description of the setup

The setup employed in the experimental demonstrations is depicted in Fig. 2. The continuous-wave light (CWL) generated by the seed laser (NKT Koheras Basik X15) is divided in two branches, acting as carriers for the probe and LO combs. The electrical combs are designed offline as a double sideband real signal and generated by two channels of an arbitrary waveform generator (AWG, M8195A Keysight). The electrical combs drive two Mach-Zehnder modulators (MZM) (set at the minimum transmission point) that modulate the carrier. A parabolic spectral phase is applied to the LO comb lines to expand the pulsewidth almost to the repetition rate of the signal [13]. To prevent arbitrary spectral phase in the beatnotes employed to reconstruct the backscattering signal, the spectral phase applied to the $\left[(p-1)M+1, pM\right]$ lines of the probe comb must match with the phase allocated on p-line of the LO [9]. The optical probe comb is amplified by an erbium-doped fiber amplifier (EDFA) and then filtered by a dense wavelength division multiplexer (DWDM) to reduce the amplified spontaneous emission. The resulting signal is sent to the fiber under test (FUT) through a circulator, which retrieves the backscattering signal.

A section of 2 cm of the FUT is mechanically perturbed by a shaker. In the LO comb branch, the optical signal is also amplified before coherent mixing with the amplified backscatter. The backscattering and LO combs are filtered by a tunable band pass filter (TBPF, Yenista XTM-50) to achieve a single sideband modulated spectrum with carrier suppression (SSBM-CS), aimed at ensuring a proper down-conversion of the backscatter information upon detection. The beating of the LO and backscattering signal is measured by means of a 100 MHz balanced photodetector (BPD, Thorlabs BPD 410C). In some cases, the oscilloscope (Osc.) sampling requirements are alleviated by employing a 50 MHz electrical low-pass filter (LPF, Minicircuits SLP-50+). It is worth noting that the experimental setup is basically a Mach-Zehnder interferometer, and no phase noise correction method has been

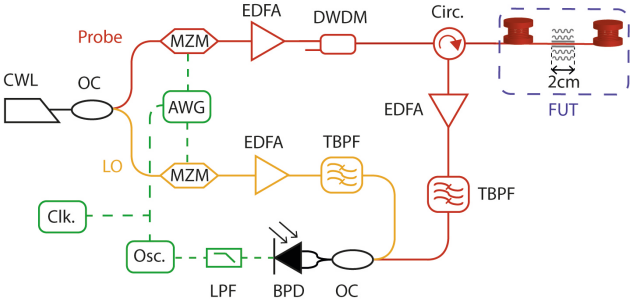

Fig. 2. Setup of the QIR-TE-φOTDR-based interrogator. OC: optical coupler, Circ: circulator. The rest of abbreviations are described in the body of the manuscript.

applied to compensate for slow phase drifts induced by vibration and temperature fluctuations between interferometer branches.

To study the influence of the frequency stability of the RF clock reference (Clk.), two RF synthesizers with different accuracy are tested. The first one was the internal AWG reference clock, based on an OCXO. The relative stability of this clock is of the order of 10^{-9}. The second clock is a rubidium oscillator linked to a GPS signal (TimeTech GPS 5.10). This clock presents a relative frequency stability of 10^{-13} in short times. In both cases, generation and digitalizing stages are synchronized (see Fig. 2).

B. Effect of the clock stability in traces.

First, we want to illustrate how the effect of the lack of accuracy in the reference clock produces a jitter that notably reduces the repeatability between successive traces. For that purpose, we designed a probe comb composed of N = 50000 lines separated 100 kHz, that allows us to measure a fiber of 1026 m of range with a spatial resolution of 2 cm. Since the QIR factor is 200, the LO comb has 250 lines. The offset between repetition rates (i.e. acoustic sampling) is 80 Hz. The employed reference clock is the OCXO, whose relative stability is worse than the required for this experiment ($\zeta_{clock} \ll 2{\cdot}10^{-10}$, according to the Eq. 11). When we send the probe signal to a FUT of 1003 meters, we retrieve a set of traces. A set of non-consecutive traces are shown in Fig. 3 a).

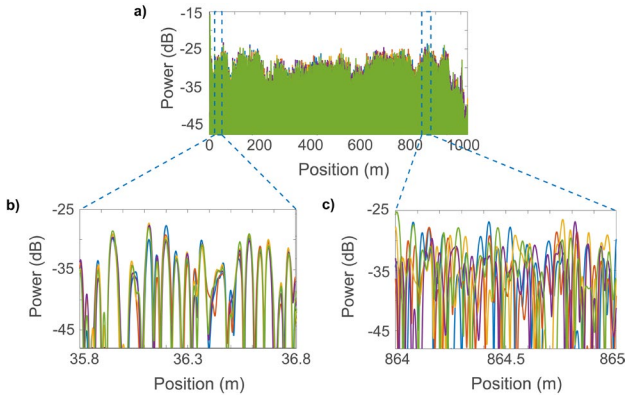

Fig. 3. Backscattered detected traces obtained from a QIR-DFC in which the probe comb is composed by N = 50000 lines separated by f_R = 100 kHz and M = 200. A window showing the structure of the trace at the beginning and the end of the trace is shown in b) and c), respectively.

Looking at the initial positions of the fiber (see Fig. 3b), we observe good repeatability between traces. However, at positions close to the end of the fiber (Fig. 3c) there is a total lack of temporal coherence between different traces. For an insufficient stability of the reference clock, integrated jitter along the trace period induces a distortion in the time-of-flight measurements, which results in the mixing of the backscattering information coming from different measurements points, particularly at large delays with respect to the trigger position.

C. Sensing results

In a first sensing experiment, we interrogate 500 m of fiber with 2 cm resolution and 1 kHz of perturbation sampling rate. Hence, the probe comb is composed of $N = 25000$ lines separated by 200 kHz. The QIR factor is $M = 320$. Therefore, the LO comb is composed of 78 lines over approximately the same optical bandwidth (5 GHz). The offset δf (corresponding to the sampling rate) is 1 kHz. The FUT has a length of 378 m. The periodic perturbation is applied over 2 cm around the 327.1 m, having a frequency of 200 Hz.

In a second experiment, the system is configured to measure up to 100,000 sensing points distributed along a maximum of 2 km with a sampling rate δf of 80 Hz. The probe comb has again 5 GHz bandwidth with a line spacing of 50 kHz. In this case, the LO has 250 lines, which corresponds to $M = 400$. The length of the FUT is 1390 m (as available in our lab), and the perturbation is applied at the 1346 m with a frequency of 10 Hz. Figure 4a and 4b show the detected traces employing the first described QIR-DFC while Fig. 4c and 4d are obtained with the second one. In Fig. 4a and 4c, the reference signal is generated with the rubidium clock, while in Fig. 4b and 4d were obtained with the OCXO (Fig. 4b and 4d). The traces in Fig. 4 a, b, c maintain the coherence along its length when the fiber is unperturbed, as it can be seen in the respective insets. However, the repeatability of the traces in Fig. 4d is lost from approximately the meter 500. This behavior, as explained above, is attributed to the lack of stability of the reference clock. In line with Eq. 11, the QIR-DFC with $N = 100{,}000$ lines requires a $\zeta_{clock} \ll 5{\cdot}10^{-11}$. Such stability is only achieved by the rubidium clock. However, for the QIR-DFC with a probe comb with $N = 25{,}000$ lines, Eq. 11 imposes a restriction of $\zeta_{clock} \ll 8{\cdot}10^{-10}$, which is easily satisfied with the rubidium clock, and barely satisfied with the OCXO clock. The phase noise induced by each reference clock also affects slightly the measured trace SNR. The SNR of the trace is calculated as the average value of the SNR obtained point-to-point over a representative interval. The point-to-point SNR value is obtained as the ratio between the mean value of the temporal evolution of the power at each point and the variance of the (temporal evolution of the) power at the mentioned point. For the first comb configuration, the SNR is 8.8 dB and 8.6 dB for the rubidium clock and the OCXO, respectively. To obtain the value, we averaged the SNR values of the section 25 m-300 m. Regarding the second comb, the

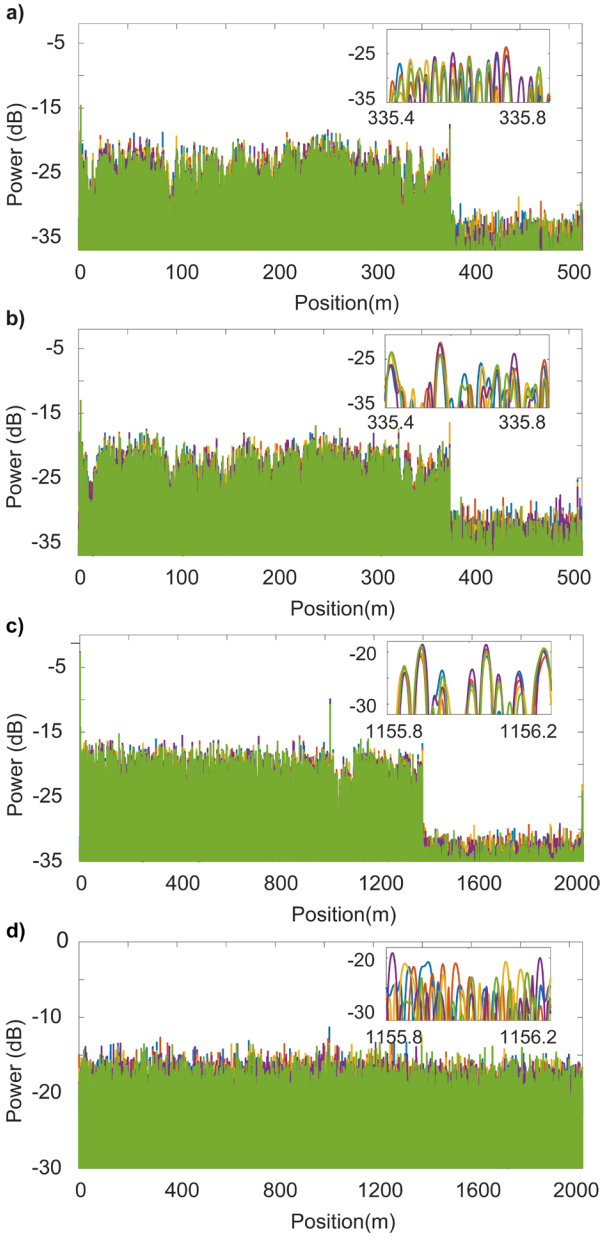

Fig. 4. Time-expanded traces recovered after spectral re-ordering employing a QIR-DFC with f_R = 200 kHz and M = 320 (a,b) and f_R = 50 kHz and M = 400 (c,d). The rubidium clock has been employed in (a) and (c), while the OCXO is applied in (b) and (d). Insets show a zoom of an unperturbed region around the end of the traces to show repeatability.

SNR with the rubidium clock is estimated in 11.5 dB, while employing the OCXO the SNR is 1.05 dB (averaged section 25m-1200 m). In all cases, we averaged a set of 0.5 s of traces. Note that the first QIR-DFC interrogates the fiber more than six times faster than the second, so its noise level is higher.

Next, we show the effect of the clock stability in the strain map around the perturbed area. Figures 5a and 5b show the evolution of the strain by using the comb with 25,000 lines. The phase in fading points is estimated based on nearest neighbor analysis [16]. Although in both cases it is possible to identify a perturbation of 200 Hz, the perturbation recovered with the OCXO clock (Fig. 5a) extends beyond the 2 cm

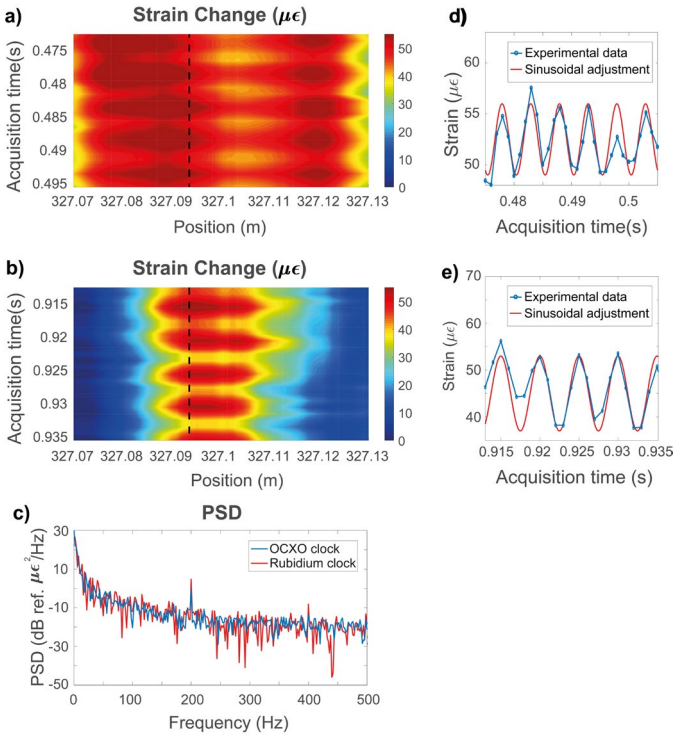

Fig. 5. Temporal evolution of the strain map around the perturbed section for the first dual-comb configuration (with N = 25,000) employing the OCXO reference clock (a) and the rubidium clock (b). The PSD for a representative perturbed point is shown in c). The temporal evolution of the strain in such point is shown in blue in d) and e). The sinusoidal adjustment of the resulting waveform sampled at 10 kHz is shown in red line.

resolution with a non-uniform amplitude. This "smearing" effect of the perturbation is attributed to the jitter of the AWG clock, which implies that there is some crosstalk between closely-reordered time samples. It should be noticed that, under small amplitude variations, broadening of the linewidth of the combs' teeth due to the perturbation can be considered negligible as compared with the broadening caused by the clock instability. In contrast, when using the rubidium clock (Fig. 5b), the perturbation is well resolved both in time and in length and the nominal resolution is achieved. Figure 5c shows the PSD of one representative perturbed point (marked with dashed lines) of the Fig. 5a (blue) and 5b (red). Both curves show a second harmonic, due to the non-linear behavior of the shaker. The estimated noise floor, calculated as the median between 420 Hz and 470 Hz, is -18.8 and -21.7 dB ref. 1 $\mu\varepsilon^2$/Hz, respectively. The median standard deviation of the measurements is 0.3 rad for both measurements, which corresponds with 1.5 $\mu\varepsilon$. The temporal strain evolution at the representative position marked by the dashed lines in Fig. 5a and 5b is shown in blue lines in Fig. 5d (OCXO) and 5e (rubidium). The sinusoidal adjustment of the resulting waveform, sampled at 10 kHz, is shown in red. The amplitude of the sine wave applied is 3.5 $\mu\varepsilon$ and 8 $\mu\varepsilon$ for Fig. 5d and 5e, respectively. The difference in the amplitude of the sinusoidal signals is probably related to a bad recovery of the phase information when the reference signal came from the OCXO clock.

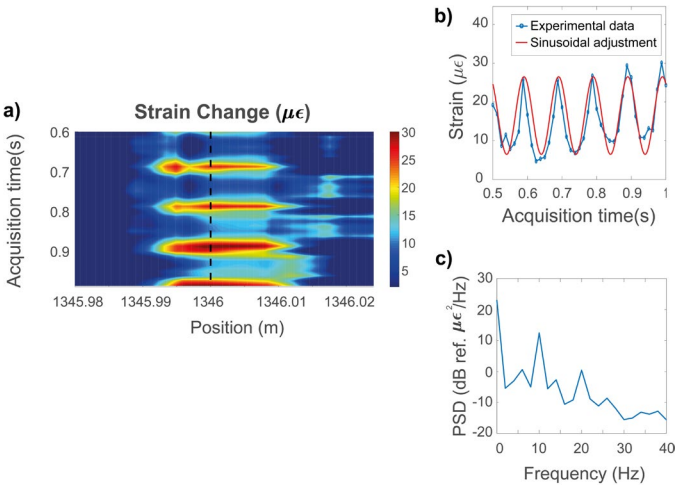

Fig. 6. a) Dynamic strain map around the perturbation for the dual-comb with N = 100000 lines employing the rubidium clock as reference. b) Temporal evolution of the strain in a representative point: experimental measurement in blue and sinusoidal adjustment in red. c) The PSD at that representative point.

Regarding the second comb, only the strain map obtained when using the rubidium clock is shown in Fig. 6a. As before, it is possible to observe a well-defined perturbation of 2 cm with a frequency of 10 Hz. The estimation of the phase in fading points is made as in the previous measurements. The strain change in a representative point is shown in blue in Fig. 6b, while the red line corresponds to the theoretical signal sampled at 80 Hz. According to the theoretical lines, the amplitude of the strain signal is 16.5 $\mu\varepsilon$. The PSD (Fig. 6c) also shows a second harmonic. In this case, the noise floor calculated between 25 Hz and 35 Hz is -11.5 dB ref. 1 $\mu\varepsilon^2$/Hz , while the median standard deviation is 0.15 rad, which corresponds with 770 $n\varepsilon$ (maintaining 2 cm of gauge length).

IV. Conclusions

In conclusion, we have demonstrated the influence of the stability of the RF clock synthesizer in the performance of QIR-TE-φOTDR. The maximum number of measurable points is directly related to the stability of the synthesizer employed as a clock reference. Comparing the QIR architecture with the original TE-φOTDR scheme, the frequency stability condition is more restricted by a factor of $2N$ due to the spectral lines reordering process. By using a rubidium clock (frequency stability of ~10^{-13}), we have demonstrated the possibility of enlarging the measurement range in QIR-TE-φOTDR, which now can reach up to 2 km (as limited by the repetition rate of the probe comb) while maintaining a 2 cm spatial resolution. This implies that up to 100,000 sensing points can be readily attainable with the proposed configuration, without any post processing correction. The flexibility of QIR-TE-φOTDR also allows increasing the acoustic sampling up to the kHz range, at the expense of reducing the range. This finding opens the door for the implementation of QIR-TE-φOTDR as a distributed acoustic sensor in medium-range and high-resolution applications that require a large number of resolved spatial points.

ACKNOWLEDGMENTS

We acknowledge to Dr. P. Corredera (Instituto de Óptica "Daza de Valdés", IO-CSIC) for lending us the rubidium clock used in this experiment.

M.S.A., V.D. acknowledge the financial support from the MCIN/AEI/10.13039/501100011033 and by the FSE invierte en tu futuro under contracts no. PRE-2019–087444, RYC-2017–23668. M.R.F.R. acknowledge the financial support from the MCIN/AEI/10.13039/501100011033 under contract IJC2018–035684-I, respectively.

REFERENCES

[1] Y. Muanenda, "Recent Advances in Distributed Acoustic Sensing Based on Phase-Sensitive Optical Time Domain Reflectometry," *Journal of Sensors*, vol. 2018, no. 3897873. pp. 1–16, 2018.

[2] M. R. Fernández-Ruiz, L. Costa, and H. F. Martins, "Distributed acoustic sensing using chirped-pulse phase-sensitive OTDR technology," *Sensors*, vol. 19, no. 20. pp. 1–28, 2019.

[3] Z. Zhan, "Distributed acoustic sensing turns fiber-optic cables into sensitive seismic antennas," *Seismol. Res. Lett.*, vol. 91, no. 1, pp. 1–15, 2019.

[4] D. Chen, Q. Liu, and Z. He, "108-km Distributed Acoustic Sensor with 220-p ϵ/Hz Strain Resolution and 5-m Spatial Resolution," *J. Light. Technol.*, vol. 37, no. 18, pp. 4462–4468, 2019.

[5] J. Xiong, Z. Wang, Y. Wu, H. Wu, and Y. Rao, "Long-distance distributed acoustic sensing utilizing negative frequency band," *Opt. Express*, vol. 28, no. 24, pp. 35844–35856, 2020.

[6] H. F. Martins, K. Shi, B. C. Thomsen, S. Martin-Lopez, M. Gonzalez-Herraez, and S. J. Savory, "Real time dynamic strain monitoring of optical links using the backreflection of live PSK data," *Opt. Express*, vol. 24, no. 19, pp. 22303–22317, 2016.

[7] W. Zou, S. Yang, X. Long, and J. Chen, "Optical pulse compression reflectometry: proposal and proof-of-concept experiment," *Opt. Express*, vol. 23, no. 1, pp. 512–522, 2015.

[8] Z. Wang *et al.*, "Distributed acoustic sensing based on pulse-coding phase-sensitive OTDR," *IEEE Internet Things J.*, vol. 6, no. 4, pp. 6117–6124, 2018.

[9] M. Soriano-Amat *et al.*, "Time-expanded phase-sensitive optical time-domain reflectometry," *Light Sci. Appl.*, vol. 10, no. 51, pp. 1–12, 2021.

[10] I. Coddington, N. Newbury, and W. Swann, "Dual-comb spectroscopy," *Optica*, vol. 3, no. 4, pp. 414–426, 2016.

[11] N. B. Hébert, S. Boudreau, J. Genest, and J.-D. Deschênes, "Coherent dual-comb interferometry with quasi-integer-ratio repetition rates," *Opt. Express*, vol. 22, no. 23, pp. 29152–29160, 2014.

[12] M. Soriano-Amat *et al.*, "Monitoring of a highly flexible aircraft model wing using time-expanded phase-sensitive otdr," *Sensors*, vol. 21, no. 11, pp. 1–10, 2021.

[13] M. Soriano-Amat, H. F. Martins, V. Durán, S. Martin-Lopez, M. Gonzalez-Herraez, and M. R. Fernández-Ruiz, "Quadratic phase coding for SNR improvement in time-expanded phase-sensitive OTDR," *Opt. Lett.*, vol. 46, no. 17, pp. 4406–4409, 2021.

[14] C. Deakin, Z. Zhou, and Z. Liu, "Phase noise of electro-optic dual frequency combs," *Opt. Lett.*, vol. 46, no. 6, pp. 1345–1348, 2021.

[15] C. Deakin and Z. Liu, "Noise and distortion analysis of dual frequency comb photonic RF channelizers," *Opt. Express*, vol. 28, no. 26, pp. 39750–39769, 2020.

[16] G. Tu, M. Zhao, Z. Tang, K. Qian, and B. Yu, "Fading noise suppression in Φ-OTDR based on nearest neighbor analysis," *J. Light. Technol.*, 2020.